ELSEVIER

Composite Structures 49 (2000) 435–441

COMPOSITE STRUCTURES

www.elsevier.com/locate/compstruct

Matrix cracking behavior of K3B/IM7 composite laminates subject to static and fatigue loading

Xiaogang Huang *, John W. Gillespie Jr., Rushad F. Eduljee, Zuwei Shen

Center for Composite Materials, University of Delaware, Newark, DE 19716, USA

Abstract

The matrix cracking behavior of a new high-performance thermoplastic composite material, K3B/IM7, was systematically investigated. Laminates in various grouped thickness and ply stacking sequences, $[0_2/90_2/0_2]$, $[0_2/90_4/0_2]$, and a quasi-isotropic laminate $[+45/0/-45/90]_s$ were tested under static and tension–tension fatigue loading. Depending on the stacking sequence of the laminates and the type of loading, various matrix cracking behavior were found. Under static loading, the matrix cracks were mainly close to the specimen edges. A few cracks were found to penetrate the specimen width, even when the load was large enough to break the specimen. However, under fatigue cyclic load, the edge initiated cracks propagated fully across the specimen width. Combined with the fatigue Paris Rule and considering the ply thickness and stacking sequence, the energy release rate method was applied to predict the relations between the loading strain amplitude and fatigue cycles for matrix cracking failure. © 2000 Elsevier Science Ltd. All rights reserved.

Keywords: Composite laminates; Matrix cracking; Delamination; Fatigue; Energy release rate

1. Introduction

Thermoplastic–matrix composites are now being used as structural members in the aerospace industry. An important design consideration is the matrix cracking behavior in laminates subjected to static and fatigue loadings. The subject of matrix cracking in composite laminates is well represented in the literature of composite strength analysis and structural member design [1–4]. Preliminary tests [5] have shown that Avimid K3B/IM7 composites exhibits attractive properties, such as high fracture toughness, high matrix cracking resistance, and high temperature performance, etc. Some unusual differences in their behavior from bismaleimide (X5260/G40-800 BMI) thermoset composites were observed. For example, most of the matrix cracks stayed at the specimen edges rather than propagated through the specimen width during the tension test. Even before the final specimen breakage, not many completed matrix cracks were observed in ultrasonic C-scan images. In order to investigate the first and major failure modes of K3B/IM7 laminates under real loading conditions, in this study, laminate tension tests were conducted, which included initial matrix crack detection, matrix cracking evolution observation, and ply delamination determination. Optical microscopy and ultrasonic polar backscatter C-scanning were used as the main tools in determining the matrix crack growth. Since the matrix cracking behavior of K3B/IM7 was more irregular than that of BMI laminates, attention was placed on matrix cracking evolution details following the crack initiation during the tests. The loading condition was extended from static tension to tension–tension fatigue. Quasi-isotropic laminate specimens were used to identify the ply lay-up effects on the matrix cracking damage.

2. Experimental

Composite laminates used for testing were prepared by filament winding of K3B/IM7 prepreg manufactured by the DuPont company. Unidirectional sheets were removed from the mandrel and cut into plies of the desired size and orientation. The panels were heated at 0.5°C/min to 360°C and held isothermally for 1 h under 13 MPa autoclave pressure. Then the panels were cooled down at 1°C/min to room temperature. Initially, a reduced vacuum level of 13 cm Hg was used and full vacuum (82 cm Hg) was applied when the temperature reached 176°C. As a result of the large amount of solvent in the Avimid K3B/IM7 prepeg, a surface bleeding

* Corresponding author.

0263-8223/00/$ - see front matter © 2000 Elsevier Science Ltd. All rights reserved.
PII: S0263-8223(00)00078-7

bagging technique was used during processing. The details of processing can be found in [6]. The unidirectional lamina mechanical properties are listed in Table 1. Laminates were initially fabricated as 30×30-cm plates, then cut into 20×2-cm specimens using a diamond saw. Care was taken to insure that excessive heating of the material did not occur during the cutting process. The end tabs on the specimens were made of fiber-glass reinforced material. Three lay-ups: $[0_2/90_2/0_2]$, $[0_2/90_4/0_2]$, and $[+45/90/-45/0]_s$ were prepared. In order to observe the details of the testing specimen, one edge of the specimen was polished with sandpaper of 3 μm diamond paste until the fibers in the bulk matrix could be clearly identified under the optical microscope.

The tension tests were conducted using a tension load frame. Mechanical data were measured through the load cell and a strain gage at the center of the specimen and recorded with the aid of a data acquisition system. At each loading strain interval, the specimen was taken from the load frame for matrix cracking inspection.

A robotic ultrasonic inspection system [7] was used to detect the initiation and evolution of matrix crack. Instead of moving the transducer normal to the specimen's surface, the transducer is moved across the specimen at an angle of 30° to the normal. The vertical matrix cracks act as a reflector and return an increased signal to the transducer. These reflections can then be easily projected in a two-dimensional image. The ultrasonic polar backscatter scanning on these specimens was performed with a spherically focused 15 MHz transducer. More details of the test procedure can be found in [8,9].

3. Static tension test

The initial matrix crack under static tension load was observed on the edge of the specimen. The first edge matrix cracks were found at an applied strain of 0.5% for $[0_2/90_4/0_2]$ and 0.6% for $[0_2/90_2/0_2]$ at room temperature. With increasing load, more cracks occurred unevenly distributed along the length of the specimen.

Table 1
K3B/IM7 composite[a]

Lamina properties	
E_L (N/m^2)	160.4×10^9
E_T (N/m^2)	8.3×10^9
v_{LT}	0.33
v_{TZ}	0.45
G_{LT} (N/m^2)	4.7×10^9
G_{TZ} (N/m^2)	3.4×10^9
α_L 1/°C	0.27×10^{-6}
α_T 1/°C	30.6×10^{-6}
t (μm)	142
G_{IC} (J/m^2)	256
T_g (°)	302

[a] The data were adopted from Ref. [5].

These matrix cracks remained at the edge area instead of propagating inward (along the specimen width). Up to the 0.9% strain, approximately 15 cracks per centimeter were found quite evenly spaced along the edge. No full-width cracks were scanned for each tested specimen. As the strain increased to 1.2%, a few full-width cracks were observed in the specimen through polar backscatter scanning. Subjected to this high strain, around 22 edge cracks per centimeter already existed in the $[0_2/90_4/0_2]$ specimen as shown in Fig. 1. By cutting the specimen along the mid-line, it was shown that the cracks in the mid-plane were much less than those in the free edge area at a ratio of 1 to 22. This static behavior of K3B/IM7 specimens is very different from that of other composite materials, such as BMI composites, in which full-width matrix cracks developed immediately after crack initiation [9].

A similar situation was found in the $[+45/0/-45/90]_s$ quasi-isotropic laminate. At around 0.55% applied strain, matrix cracks in the 90° layer were found using optical microscopy. More cracks developed as the load increased, but they remained in the edge areas. As the strain reached 0.7%, approximately 14 cracks per centimeter were found along the edge of specimen. At an applied strain of 0.9%, a few full width matrix cracks were shown through polar backscatter scanning. In edge areas of the ±45° layers of tested specimens, only a few matrix cracks could be observed at an applied strain level of 1%.

4. Tension–tension fatigue tests

Tension–tension fatigue tests were performed in a servo-hydraulic testing machine. The load frame was operated under applied strain control mode with a frequency of 1 Hz. Various constant strain amplitudes with $R = 0.01$ ($R = \varepsilon_{min}/\varepsilon_{max}$) were applied (see Fig. 2). Cross-ply $[0_2/90_2/0_2]$, $[0_2/90_4/0_2]$ and quasi-isotropic $[+45/0/-45/90]_s$ specimens were fatigued first at crack initiation strain levels (based on static tests). At each cyclic interval, the specimen was unloaded and inspected through microscopy and polar backscatter C-scanning. Under constant strain amplitude cyclic loading, the initial matrix cracks in the free edge gradually propagated to the center of specimen. Fig. 3 shows C-scan images of the matrix crack propagation due to fatigue loading for $[0_2/90_4/0_2]$ laminates at a strain amplitude of 0.5%. In the first 500 cycles, an edge crack starts to propagate along the width direction of the test coupon. With increasing fatigue cycles, more cracks were formed. At up to 10,000 cycles, a fully developed crack density at 2–3 cracks per centimeter was observed. With further increased cycles, a higher crack density was found in the form of full-width cracks.

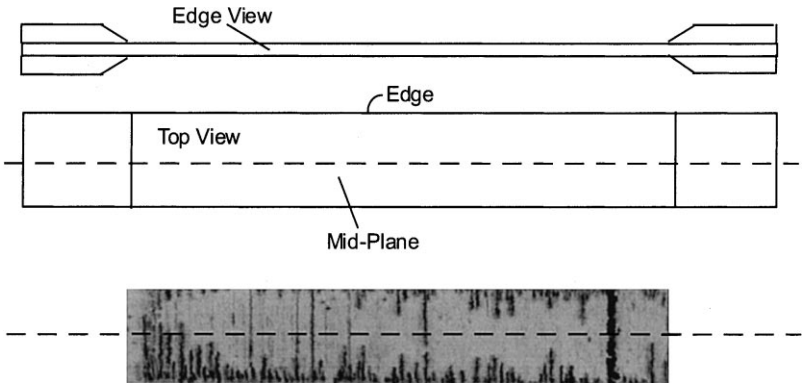

Fig. 1. Matrix cracking subjected to static tension strain 1.2% for $[0_2/90_2/0_2]$ specimen.

The specimens were then loaded at lower strain amplitudes. After 80,000 cycles at 0.4% strain, the first full matrix crack was found in the 90° layers. With decreasing strains, the number of cracking cycles significantly increased. In the case of decreasing strain amplitude to 0.3%, the critical onset cycle number was increased to 600,000. The same test procedures were performed for $[0_2/90_2/0_2]$ specimens. Three testing coupons were used at each strain amplitude to give an average onset value of matrix crack initiation and subsequent multiple crack evolution under fatigue cycles. Fig. 4(a)–(c) plot the fatigue strain amplitudes for critical fatigue cycles of initial matrix cracking for $[0_2/90_2/0_2]$, $[0_2/90_4/0_2]$, and $[+45/0/-45/90]_s$ laminates, respectively. From these curves, the uncracked zones can be determined as a function of applied strains and fatigue cycles.

After an initial crack formed, the crack growth and evolution were of primary concern. The $[0_2/90_2/0_2]$ laminate specimens were subjected to continued fatigue at 0.5% strain amplitude after the initiation cycles. Meanwhile, each specimen was unloaded periodically inspected to determine the number of cracks throughout the gage length. As the cyclic number increased, more edge cracks propagated into fully developed cracks along the specimen width. After 100,000 cycles, a significant crack density of 14 full cracks per centimeter was achieved. Up to 400,000 cycles, a saturation level of crack density was obtained of 22 cracks per centimeter for the $[0_2/90_2/0_2]$ laminate. With decreasing applied load, a higher cyclic number is needed to form multiple matrix cracks in the 90° layers. In this way, the relationship between crack density and cyclic number was obtained. Fig. 5(a) and (b) show the multiple matrix cracking developments for cross-ply $[0_2/90_4/0_2]$ and $[0_2/90_2/0_2]$ laminates. Before matrix cracking reached saturation, there were no obvious delaminations along the 90°/0° interfaces for both kinds of specimens.

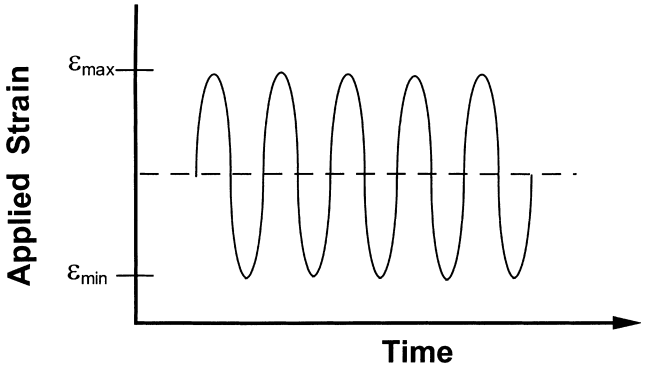

Fig. 2. Schematic of tension–tension fatigue loading.

5. Observation of quasi-isotropic laminate fatigue damage growth

In practice, laminates are used in the form of quasi-isotropic laminates. Special attention was placed on monitoring the fatigue damage growth in quasi-isotropic laminate specimens. The initial fatigue test was conducted at 0.4% strain amplitude. Full cracks started to appear in the 9° layers after 10,000 cycles and became wider after 100,000 cycles. Only a few edge cracks appeared in the ±45° layers. Delaminations formed between the −45° and 90° layers after 150,000 cycles but were still very small at that stage. Most of these local small delaminations were located around full matrix crack tips. After 250,000 cycles, the delaminations became longer (up to 2–4 ply thickness in length) and thicker. Around 400,000 cycles, most of these individual delaminations connected together along the 90°/−45° interface.

By increasing the strain amplitude to 0.5%, a few small cracks began to appear along the specimen edge in 90° layers at 2000 cycles. The cracks grew in thickness and width with increasing loading. Up to 200,000 cycles, the transverse cracks reached saturation level (24 cracks per centimeter). The local delaminations near the transverse crack tips between the 90° and 45° layers at

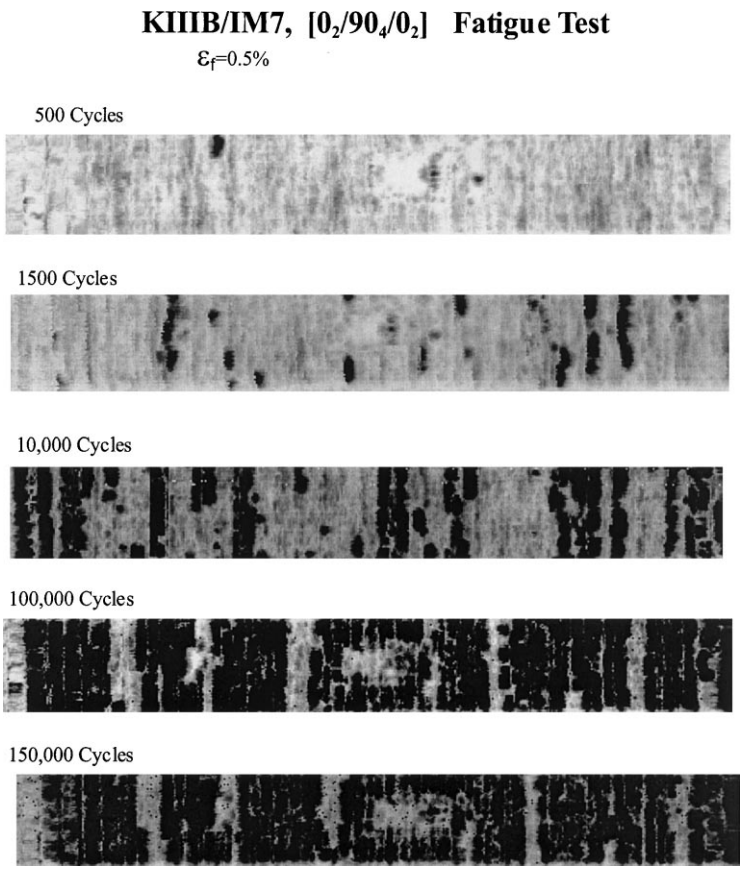

Fig. 3. Matrix cracking evolution under tension–tension fatigue loading.

around 120,000 cycles spread rapidly along the layer interfaces and formed larger cracks. At 300,000 cycles, the separations of the 90°/−45° layers were found in most of the layer interfaces.

With further increasing the strain amplitude to 0.6, full-matrix cracks started developing after only 300 cycles. By 5000 cycles, multiple transverse cracks at a density of 4 cracks per centimeter were found. Delaminations between 90° and −45° layers were observed at approximate 20,000 cycles, which was much earlier than in tests run at lower strain amplitudes. By 100,000 cycles, significant delaminations and transverse cracks developed and joined to form widespread damage in the matrix and interfaces. From these testing results, it was seen that after certain cycles, full transverse cracks in the 90° layer formed first, then more cracks developed to yield higher crack densities. With further increasing cycles, the transverse cracks acted as local defects causing localized interlaminar stresses. The delaminations extended and connected with each other. These delaminations grew with the increasing cycling load and their coalescence precipitated a massive 90°/45° interface separation. This last event is believed to cause significant laminate stiffness and strength reductions. Summarized test results of specimens subjected to 0.4–0.6% strain amplitudes are displayed in Fig. 6.

6. Analysis of cycling during fatigue loading

Extensive investigation has been done [1–4,9–13] in the area of modeling of matrix cracking. The fatigue simulation can be extended based on the static analysis. It is believed that the physical source of multiple matrix cracks is attributed to inherent material defects or flaws [14]. The condition for the flaw to propagate into a matrix crack is given by the Griffith criterion [15]

$$G(\varepsilon, a) = G_{\mathrm{IC}}, \tag{1}$$

where G_{IC} is a material toughness property against matrix rupture, which is determined by phenomenological experiments, and $G(\varepsilon, a)$ is a mathematical quantity, the energy release rate, which is a function of applied strain ε and flaw size.

In the static case, the assumption of effective flaws [16] in the 90° layer of cross-ply laminates smoothes out the microscopic effect of the real material defects. The composite laminate is assumed to contain randomly distributed effective flaws whose identity and distribution are simply presumed known. Under certain loading conditions, some dominant micro-flaw or a cluster of such flaws will become critical and initiate matrix cracking on the macro-scale. The model is described mathematically by the method of fracture mechanics, in

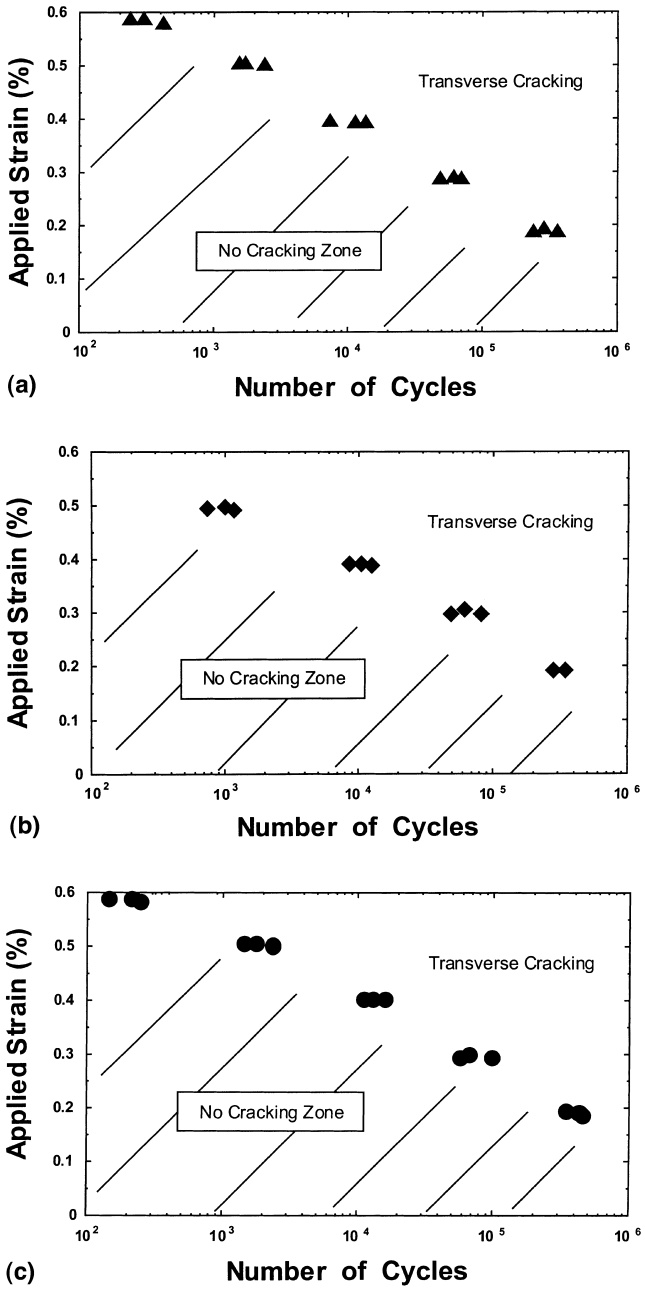

Fig. 4. (a) Initial matrix cracking in 90° plies for $[0_2/90_2/0_2]$ laminates in ε_f–N space; (b) initial matrix cracking in 90° plies for $[0_2/90_4/0_2]$ laminates in ε_f–N space; (c) initial matrix cracking in 90° plies for $[+45/0{-}45/90]_s$ laminates in ε_f–N space.

conjunction with a quasi-three-dimensional finite element crack-closure procedure [17]. The critical condition is provided by the energy release rate criterion. In the same manner, matrix cracking subjected to cyclic fatigue loading can be similarly described, so that the effective flaw grows continuously with each cycle of the fatigue loading. In this regard, the strain energy release rate associated with the flaw under stress will be regarded as the growth driving force. The specific flaw growth rate per cycle is assumed to follow the power rule [18]

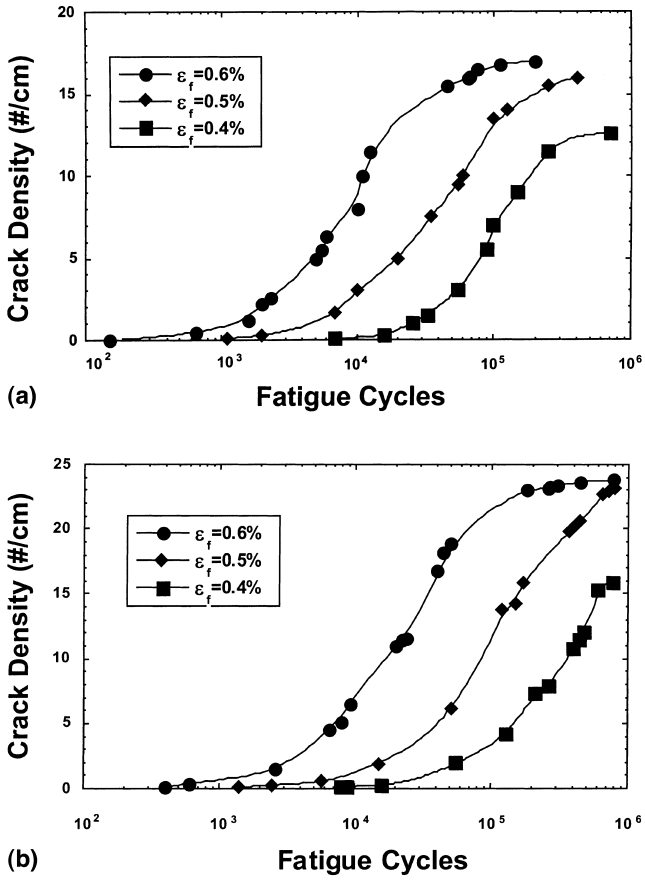

Fig. 5. (a) Matrix crack density development in 90° plies of $[0_2/90_4/0_2]$ laminate; (b) matrix crack density development in 90° plies for $[0_2/90_2/0_2]$ laminate.

$$\frac{da}{dN} = \alpha \left[\frac{G(\varepsilon_f, a)}{G_{IC}} \right]^p, \tag{2}$$

where a is the flaw size, N the fatigue cycle number, ε_f the strain amplitude, G_{IC} the material fracture toughness and α, p are material parameters.

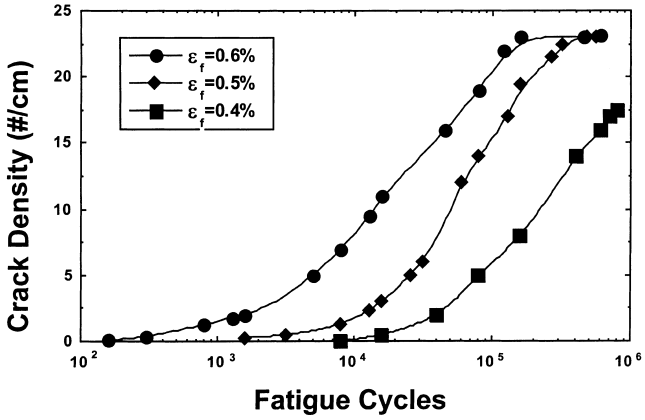

Fig. 6. Matrix crack density development in 90° plies of $[+45/0/-45/90]_s$ laminate.

The calculated energy release rate G can be expressed explicitly in terms of applied strain ε_f

$$G(\varepsilon_f, a) = C_e(a)\varepsilon_f^2 t, \tag{3}$$

where t is the ply thickness and $C_e(a)$ is a coefficient function dependent on the crack sizes, and material properties of the laminate.

If the laminate is subjected to processing cure temperature drop ΔT only, the residual thermal stresses surrounding the flaw tip also cause crack growth. The associated energy release rate G due to ΔT is

$$G(\Delta T, a) = C_t(a)\Delta T^2 t, \tag{4}$$

where C_t is a coefficient function similar to C_e, and in addition, also dependent on the thermal expansion mismatch between longitudinal and transverse directions.

By considering both mechanical load and temperature load, the energy release rate G is expressible as

$$G(\varepsilon_f, \Delta T, a) = [\sqrt{C_e}\varepsilon_f + \sqrt{C_e}\,\Delta T]^2 t. \tag{5}$$

The critical crack length of K3B/IM7 is approximately $0.75t$. When C_e and C_t curves be generated by finite element method, this critical length can be identified, which causes the largest energy release rate. The details of theory verification and computation procedure for C_e and C_t are found in [[19], Appendices A and B; [20]].

Since $G(\varepsilon_f, \Delta T, a)$ can be expressed as a continuous function of flaw size a, the equation can be integrated with respect to the flaw size until it reaches the 90° layer thickness t. The number of cycles needed to propagate the flaw size a to the transverse crack (size t) can be found as

$$N = \int_a^t \frac{1}{\alpha\left[\frac{G(\varepsilon_f, \Delta T, a)}{G_{IC}}\right]^p} \mathrm{d}a. \tag{6}$$

When a flaw has grown to size t, a transverse crack is defined. N is regarded as the initial cycle for transverse crack under the strain amplitude ε_f. The constants α and p are assumed to be material related properties; as such, these can be determined through the experimental correlation study. In the simulation, adjustment of the chosen parameters α and p were repeated many times until a satisfactory comparison with experimental results was obtained. The parameter α controls the number of fatigue cycles for the same loading amplitude. The influence of p affects the rate of the flaw growth. A lower p corresponds to a steeper damage–fatigue cycle curve. The simulation routine described above can provide a matrix cracking damage state in the laminate at any given cycle N for a constant amplitude fatigue load ε_f. The functional relationship between the strain ε_f and the cycle number N is generated numerically and plotted as a critical continuous curve in $G(\varepsilon_f$–$N)$ space. The simulations for the three types of tested specimens were plotted in Fig. 7 (a)–(c). The simulation curves for the matrix crack initiation nicely matched the testing data for the $[0_2/90_2/0_2]$, $[0_2/90_4/0_2]$, and $[+45/0/-45/90]_s$ specimens, respectively. The cyclic number increased significantly as the loading strain decreased. From the correlation of the simulation and testing data, α was found to be $0.007t$ and p was 8.5.

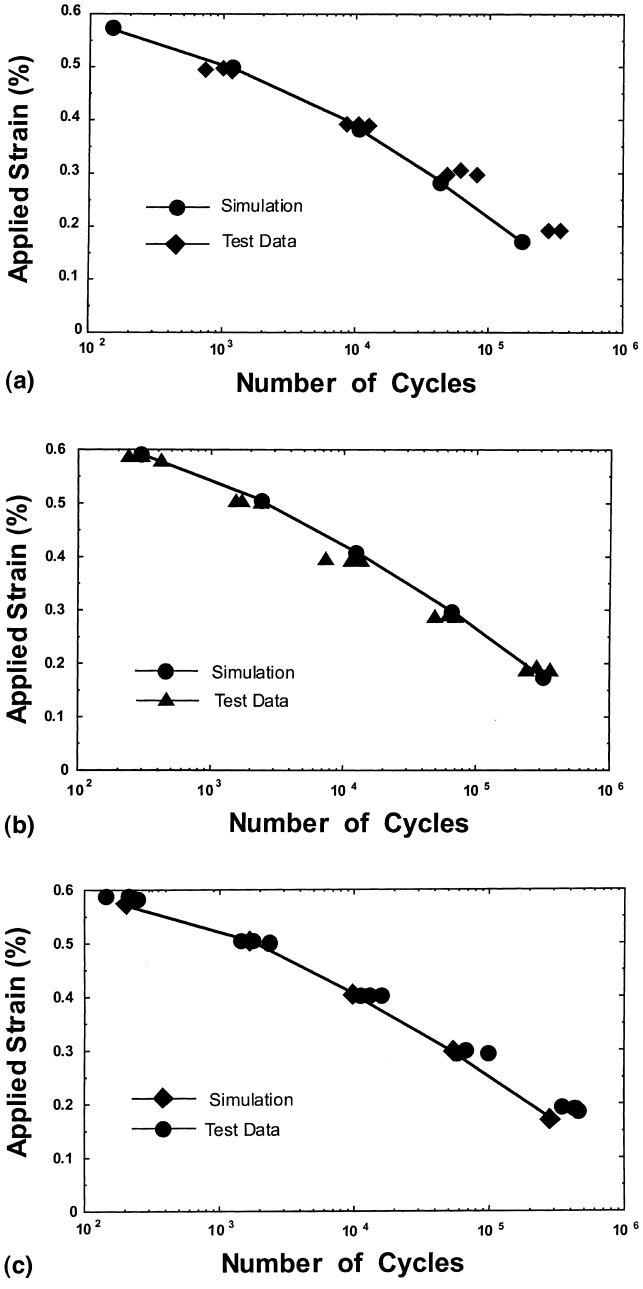

Fig. 7. (a) Comparison of fatigue simulation and test data of initial matrix cracking for $[0_2/90_4/0_2]$ laminate; (b) comparison of fatigue simulation and test data of initial matrix cracking for $[0_2/90_2/0_2]$ laminate; (c) comparison of fatigue simulation and test data of initial matrix cracking for $[+45/0/-45/90]_s$ laminate.

7. Summary

Three types of K3B/IM7 laminate specimens were tested under static and fatigue loading for sublaminate damage growth. Under static loading, the matrix cracks occurred in the 90° layers first and remained in the specimen edge area. With increasing of the load, more 90° edge cracks occurred but still in the edge area. Only under fatigue loading, the edge cracks would expand inward to form the full-width cracks. After crack initiation, the loading cycle is the main factor causing propagation of local cracks. High full-width crack densities were developed with further fatigue, and local delaminations followed the high-density cracking. For the various ply lay-up specimens, $[0_2/90_2/0_2]$, $[0_2/90_4/0_2]$, and $[+45/0/-45/90]_s$, the failure mechanisms under fatigue loading are similar. The 90_2 layer has higher matrix cracking resistance than the 90_4 layer. This is attributed to different 90° layer thickness (90_2 and 90_4) and interface (90°/45° and 90°/0°) constraining effects. The thicker the specimen, the lower will be the onset cracking strain. The weaker the layer constraint, the easier it is for ply delamination to occur.

A power-type fatigue growth approach was applied to describe 90° layer crack development and support the testing. Correlation between the experiments and the simulation under static and constant amplitude fatigue loads has been discussed. The parameters (α and p) necessary to characterize the crack fatigue growth rule have been determined by correlating the experimental results with the simulations. Comparisons between the verification tests and simulation results have also been presented.

Compared with the static studies, the fatigue study yields further understanding of the K3B/IM7 laminate damage mechanism. Matrix cracking depends on applied load and loading fatigue cycles. In the high fatigue cycle situation, small strains (lower than critical initiation strain) can also cause serious matrix cracking damage in the specimens. In the design of K3B/IM7 composite material structures, both material static and fatigue strength should be considered.

References

[1] Hashin Z. Analysis of stiffness reduction of cracked cross-ply laminates. Eng Fract Mech 1986;25:771–8.
[2] Nairn JA. Microcracking, microcrack-induced delamination, and longitudinal splitting of advanced composite structures. NASA Contractor Report 4472. Contract NAS1-18833, November 1992.
[3] Crossman FW, Wang ASD. The dependence of transverse cracking and delamination on ply thickness in graphite/epoxy laminates. ASTM STP 1982;139:118–39.
[4] Adams DS, Herakovich CT. Influence of damage on the thermal response of graphite–epoxy laminates. J Therm Stress 1984;7:91–101.
[5] Huang XG, Gillespie JW Jr., Eduljee R. Fracture test and prediction of high speed civil transport composite materials, In: Proceedings of the Eighth ASC Technical Conference in Cleveland, October, 1993;573–82.
[6] Du Pont company, fibers department, Vacuum Bag layup on graphite tooling for Avimid K Prepregs, 1990.
[7] Steiner KV, Eduljee RF, Huang XG, Gillespie Jr JW. Ultrasonic NDE techniques for evaluate matrix cracking in composite laminates. Comp Sci Tech 1995;53:193–8.
[8] Huang XG, Morin S, Gillespie JW Jr., Eduljee R. Experiment tests on composite matrix cracking by acoustic emission, Ultrasonic C-scan and replica tape techniques, In: Proceedings of the 25th International SAMPE Technical Conference in Philadelphia;1993:542–51.
[9] Huang XG, Gillespie JW Jr., Eduljee R. Matrix cracking of high-performance composite laminates with variation of laminate stacking sequence and testing temperatures. ASTM, Compos Technol Res 1997;19 (3).
[10] Lavergood RE, Ishai O. The mechanical performance of cross-plied composites. Polym Eng Sci 1971;11:226–32.
[11] Parvizi AK, Garrett W, Bailey JE. Constrained cracking in glass fiber-reinforced epoxy cross-ply laminates. J Mater Sci 1978;13:195–201.
[12] Garrett KW, Bailey JE. Multiple transverse fracture in 90° cross-ply laminates of a glass fiber-reinforced polyester. J Mater Sci 1977;12:157–68.
[13] Wang ASD. Fracture analysis of matrix cracking in laminated composites. NADC-85118-60. Naval Air Development Center, Warminster, PA, 1985.
[14] Wang ASD, Chou PC, Lei SC. A stochastic model for the growth of matrix cracks in composite laminates. J Comp Mater 1984;18:239–54.
[15] Griffith AA. The phenomena of rupture and flow in solids. Philos Trans R Soc 1920;221:163–98.
[16] Wang ASD, Crossman FW. Initiation and growth of transverse crack and edge delamination in composite laminates: part I. An energy method. J Comp Mater 1980;14:71–87.
[17] Wang ASD, Barsoum M, Haung XG. Matrix cracking initiation in brittle matrix composites: experiment and predications. In: Proceedings of the Symposium on High Temperature Composites. Amer Soc Comp. Lancaster (PA): Technomic, 1989. pp. 166–75.
[18] Paris PC, Johnson HH. Sub-critical flaw growth. Eng Frac Mech 1968;1:3–15.
[19] Gillespie JW Jr., Huang XG, Hansen U. Modeling approach for the effects of high temperature on long-term performance composites. Technical Report 92-03. Center for Composite Materials, University of Delaware.
[20] Lei S, Wang ASD. A comprehensive study on damage tolerance properties of notched composite laminates. Drexel University annual scientific report, September 1985.